Earth Sciences
2018; 7(4): 175-182
http://www.sciencepublishinggroup.com/j/earth
doi: 10.11648/j.earth.20180704.15
ISSN: 2328-5974 (Print); ISSN: 2328-5982 (Online)

Characteristics of Convective Storm Top Altitudes in Summer over the Tibetan Plateau by GPM

Cai Hongke[1], Sun Yi[1, 2], Chen Quanliang[1, *]

[1]School of Atmospheric Sciences, Chengdu University of Information Technology, Plateau Atmospheric and Environment Laboratory of Sichuan Province, Chengdu, China

[2]Guizhou Meteorological Observatory, Guiyang, China

Email address:

caihk@cuit.edu.cn (Cai Hongke), chenql@cuit.edu.cn (Chen Quanliang)

[*]Corresponding author

To cite this article:

Cai Hongke, Sun Yi, Chen Quanliang. Characteristics of Convective Storm Top Altitudes in Summer over the Tibetan Plateau by GPM. *Earth Sciences*. Vol. 7, No. 4, 2018, pp. 175-182. doi: 10.11648/j.earth.20180704.15

Received: July 19, 2018; **Accepted**: August 3, 2018; **Published**: August 29, 2018

Abstract: To have a clear understanding of the convective precipitation over the Tibetan Plateau (TP) and its surrounding regions, this research systematically studied characteristics of distribution of convective storm top altitudes over the Tibetan Plateau and its surrounding regions by using the level-2 orbital data obtained by the Global Precipitation Mission (GPM) Dual-frequency Precipitation Radar (DPR). The following conclusions are drawn in this study. (1) Because of the development of Asia summer monsoon, the number of samples of precipitation with storm top altitude above 10 km increases gradually from June to August, and all the samples of precipitation diminishes with the increases of altitude. That is, the higher the storm top altitude, the less the frequency of precipitation. (2) The deep convection frequency above 10 km altitude over the Tibetan Plateau and its surrounding regions is less than 0.8%. The deep convection frequency above 14 km is obviously less than the 10 km deep convection, not exceeding 0.2%. (3) With the increase of convective storm top altitude, the proportion of corresponding deep convection decreases exponentially. The contribution of convective precipitation to total precipitation is consistent with the contribution of convective precipitation frequency to total precipitation frequency, and the both area fractions of them decrease rapidly with the increases of the contribution. Besides, both of the two maximum contributions are below 40%. (4) The storm top altitude and surface rain rate of convective precipitation are the lowest in June and the highest in August. Furthermore, the storm top altitude over the TP rises slowly from the western part of the plateau to the eastern part, and the rain rate shows a significant gradient change with the increases of height. Below 6 km altitude, the maximum value of rain rate can reach 8 mm/h, but the precipitation intensity reduce to 4 mm/h when the altitude is above 6 km.

Keywords: GPM DPR, Tibetan Plateau, Convective Precipitation, Storm Top Altitude

1. Introduction

The altitude of the storm top is known as the maximum height of the precipitation cloud top detected by the precipitation radar in the precipitation cloud, which is related to the strength of the updraft and atmospheric stability [1]. The height of the storm top is usually related to the wavelength of the precipitation, the longer the wavelength of radar and precipitation radar, the lower the detected storm height. On the other hand, the storm top altitude always corresponds to the strong updraft in the thicker clouds at the top of clouds, which usually produces heavier precipitation [2, 3]. The Asian monsoon region is one of the regions with frequent convective activity in the world, especially over the South Asian monsoon regions. Strong convective activity not only leads to the differences of distribution of various atmospheric components, such as water vapor, in the upper troposphere, but also will cause low concentrations of ozone from the lower troposphere to enter the upper troposphere and the lower stratosphere (UTLS) region [4]. The sever convection will also affect the process of air pollutants generated from ground rising to the stratosphere. Therefore, the air in the UTLS has the characteristics of tropospheric and stratospheric atmosphere at the same time [5]. Accompanied by the deep convection, Li et al. [6] pointed out that the air pollutants released from South

Asia and southern China are uplifted to the upper troposphere under the action of early westward-moving tropical jet in the Middle East. Furthermore, the distribution of contaminants observed by satellite shows that high concentrations of carbon monoxide exist in the upper troposphere over the South Asia in summer [7]. Gettelman et al. [8] used the global chemical model and actual observations to indicate that about 75% of water vapor flux delivered to the global tropical stratosphere occur over the South Asian monsoon and the Tibetan Plateau regions. Briefly, a strong ascending airflow in the deep convection plays an important role in the transition of air from the troposphere to stratosphere, which will affect stratospheric chemistry and troposphere-surface radiative balance [9, 10].

Due to the complexity of the terrain, the world's largest, highest elevation of the Tibetan Plateau is known as the "roof of the world" and "third pole" of the earth. Because of the scarcity of rain gauge over the plateau, it is relatively difficult to collect valid precipitation data, and thus it is little about the rainfall information over the plateau. However, the situation has changed since 1979, mainly due to the First and Second Plateau Meteorological Science Experiments (1979 and 1998), respectively, and the observations by the first satellite-borne precipitation radar (PR) on board the Tropical Rainfall Measuring Mission (TRMM), which was launched in 1997. These satellite observation data provide a convenient way to research the plateau precipitation characteristics and convective activities [11-14]. Moreover, these data surmount not only the range limitations of ground radar observation, but also the low-resolution limitations of microwave detection, which cannot obtain information in the vertical direction. Therefore, the observation of satellite-borne rainfall radar is the most effective way to reveal the temporal and spatial distribution of precipitation in the world [15, 16]. According to the observations of PR, many scholars have studied the type and distribution of precipitation over tropical, subtropical and the Tibetan Plateau regions [17-22]. Fujinami [23] analyzed the diurnal variation of convective precipitation over the southern Tibetan Plateau in summer, and pointed out that the formation and development of convective clouds were strongly influenced by the plateau terrain. TRMM PR data was used to study the characteristics of summer precipitation over the Tibetan Plateau, and showed that there existed a strong diurnal variation and that the top of a precipitation cloud was about 2 km~4 km above the surrounding terrain; in other words, the cloud formed a "tower mast" [24, 25]. Wang et al. [26] analyzed the variation of cloud water content and precipitation in different seasons over the Tibetan Plateau using TRMM 3A12 data, and found interannual variation of hydrometeors over a period of ten years; this showed a gradual decline over the northeast and northwest of the plateau, but an increase in other areas.

The above-mentioned studies are all based on PR, but the TRMM satellite has stopped the observation task in April 2015. As a follow-up satellite precipitation program for TRMM, the Global Precipitation Mission (GPM), which carried the second generation of space-borne Dual-frequency Precipitation Radar (DPR), was launched in February 2014. DPR is regarded as the major instrument boarded on the precipitation measurement core platform. DPR consists of a 13.6 GHz Ku-band radar (KuPR) and a 35.5 GHz Ka-band radar (KaPR). KuPR and TRMM PR have the same working principle, and both of them can effectively detect the heavy rainfall. Compared with KuPR, KaPR has a shorter detection wavelength, a higher sensitivity to smaller particle precipitation, and can detect weak precipitation. By combining KaPR and KuPR's detection information, DPR can effectively detect weak and heavy precipitation. Hamada and Takayabu [27] pointed out that DPR could detect 21.1% more precipitation frequency and and 1.9% more precipitation volume than TRMM PR. In addition, DPR is capable of reflecting the precipitation particle spectrum and solid precipitation, and offering about 65 degrees north and south coverage. This application of DPR provides great convenience for the further study of precipitation characteristics and spatial structure in mid-high latitudes, especially in plateau regions [28, 29].

GPM satellite has been running for more than three years. Some scholars used early DPR observations for a large number of studies, and achieved some meaningful results. Chandrasekar and Le [30] evaluated the DPR precipitation profile and bright band information. Toyoshima et al. [31] analyzed the differences of storm top altitudes between diverse precipitation products of DPR. Using TRMM TMPA 3B42 and GPM Day-1 IMERG for comparative analysis, Tang et al. [32] studied the China's southeast Ganjiang River Basin, and found that the GPM precipitation products can completely replace TRMM precipitation products, with broad application prospects. However, the application of GPM precipitation data over the Tibetan Plateau has not yet been carried out. Based on this, the characteristics of convective precipitation over the Tibetan Plateau and its surrounding areas in summer (June to August) were analyzed by using the GPM DPR_HS data from 2014 to 2016.

2. Data and Method

GPM satellite has a non-solar synchronous orbit at height of 407 km at 65° inclination. The orbital period of the satellite is 93 minutes, about 16 laps around the earth one day. GPM is not only equipped with DPR, but also carries a multi-band GPM Microwave Image (GMI). Compared to TRMM satellite, GPM's coverage is much broader, and its equipment is more advanced [16]. The data used in this study are derived from the secondary standard precipitation products of GPM DPR that are issued by GSFC/NASA (Goddard Space Flight Center, National Aeronautics and Space Administration), which display the three-dimensional precipitation information along the track.

If the storm top altitude exceeds 10 km, the convective activity detected by DPR is defined as the deep convection. And according to the altitude of storm top, this study divides the deep convection into two types of 10 km and 14 km. The storm top altitude is the absolute height above sea level in this study. Before statistical analysis, Figure 1 shows the research

area identified in this present research, including the main body of the Tibetan Plateau (elevation > 3 km) and the surrounding areas (elevation < 3 km). In order to facilitate mapping and analysis, the DPR orbital data were taken with a resolution of 0.25° × 0.25° on a latitude-longitude grid. In addition, the frequency of deep convection is defined as the ratio of the number of deep convection observed by DPR in a grid box to the total number of detection in the same grid box.

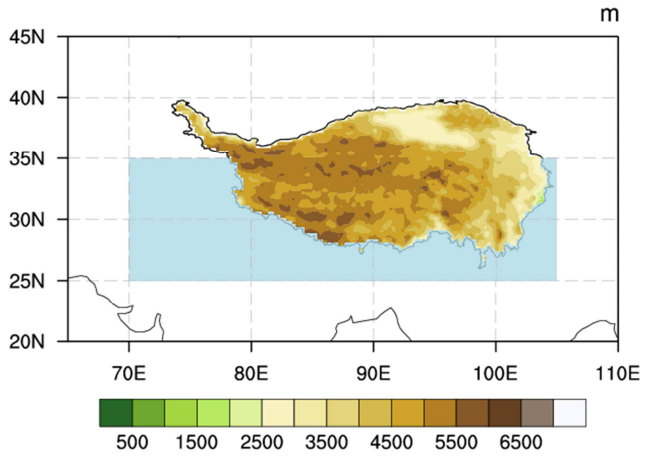

Figure 1. *The Tibetan Plateau and surrounding regions (blue).*

3. Results

3.1. Sample Statistics

Figure 2 shows the distribution of precipitation whose storm top reach 10 km in summer from 2014 to 2016 over the Tibetan Plateau and surrounding regions, where the storm top is defined as the highest level at which GPM DPR rain rate is > 0.2 mm/h, which is the lowest detectable rain rate by the instrument. The samples consist of convective precipitation, stratiform precipitation and other types of precipitation (not belonging to either of the other two categories). It can be seen from Figure 2 that the number of samples with the storm top altitude greater than 10 km are increasing from June to August, and the number of samples decrease along with height. That is-, whether it is convective, stratiform or the other type of precipitation, the higher the storm top altitude is, the less precipitation frequency occur. The number of samples over the Tibetan Plateau is larger than that over the surrounding regions in June (Figure 2a). In July (Figure 2b), the number of samples in both regions increase, but the disparities between them begin to shrink. In August (Figure 2c), both of the number of precipitation samples over the plateau and over the surrounding regions increased obviously, and the difference between them was further reduced. Throughout the summer, because of the development of Asia summer monsoon, the number of samples over 10 km over the surrounding regions is always larger than that over the plateau.

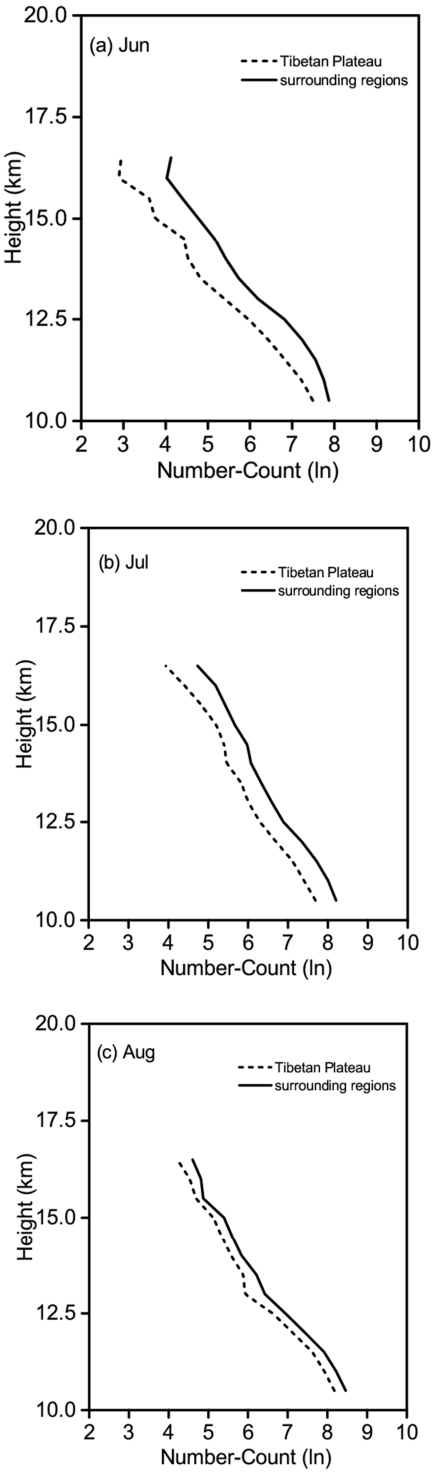

Figure 2. *Samples for different storm top altitudes that the rain rate is greater than 0.2 mm/h in June (a), July (b) and August (c) over the Tibetan Plateau and surrounding regions.*

3.2. Frequency of Convective

In order to understand the distribution of precipitation over the Tibetan Plateau and its surrounding regions, especially the convective precipitation, the frequency of precipitation is used to show the distribution of convective precipitation. This indicator could show the occurrence probability of two types

of deep convection. Since the horizontal distribution of this index can effectively indicate the regional differences of deep convection, the frequency of deep is presented in each 0.25° longitude-latitude grid box over the Tibetan Plateau and its surrounding regions (Figure 3).

Using the TRMM PR data, Liu et al. [21] analyzed the climatological characteristics of deep convection in summer over the subtropical regions, and pointed out that the areas with high frequency of deep convection mainly include the southern part of the Tibetan Plateau. It is shown in Figure 3a that the occurrence of 10 km deep convection covers the Tibetan Plateau and the surrounding regions during summer from 2014 to 2016. The occurrence of 10 km deep convection is mostly below 0.8% over the both of regions, while it is not more than 0.6% over the main body of Tibetan Plateau. The number of 10 km deep convection over the surrounding regions is higher than that over the main body of Tibetan Plateau.

Figure 3b shows the horizontal distribution of the frequency of 14 km deep convection. Compared with Figure 3a, it is not difficult to find a good correspondence between the frequency of 10 km deep convection and 14 km deep convection, but there is a distinct difference between them. First, the frequency of 14 km deep convection is significantly smaller than 10 km deep convection, which does not exceed 0.2%, and the former appears over the surrounding regions. Second, the coverage of 14 km deep convection is also obviously smaller than that of 10 km deep convection. In other words, the probability of 14 km convection is much smaller than that of 10 km convection over the Tibetan Plateau and its surrounding regions.

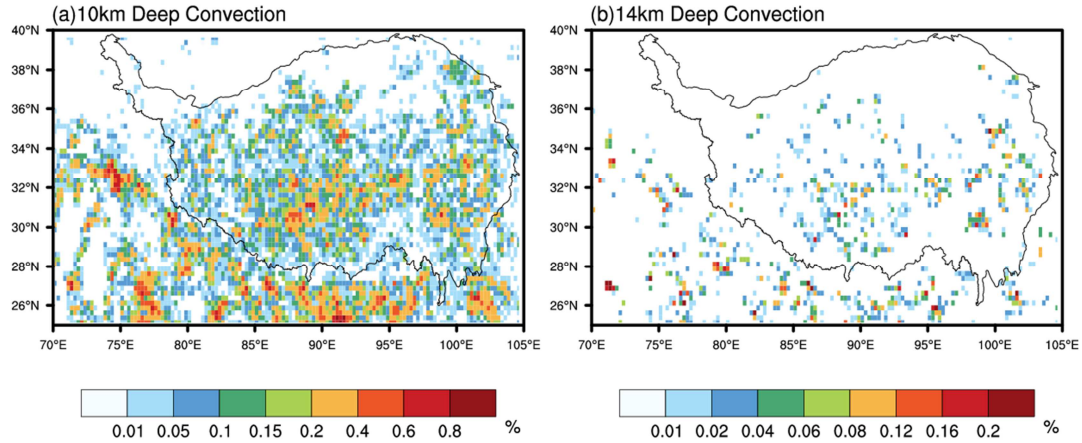

Figure 3. *Distributions of deep convection frequency over the Tibetan Plateau and surrounding regions.*

To comprehend the zonal distribution of characteristics of convective, Figure 4 shows the zonal mean of the frequency of two types of deep convection. No matter what type of deep convection, the distribution of frequency shows a bimodal model from low latitudes to high latitudes, and the smaller frequency of both of them exists in the northern Tibetan Plateau (north of 35°N). The maximum value of the frequency of 10 km deep convection and 14 km deep convective are 0.15% and 0.0154%.

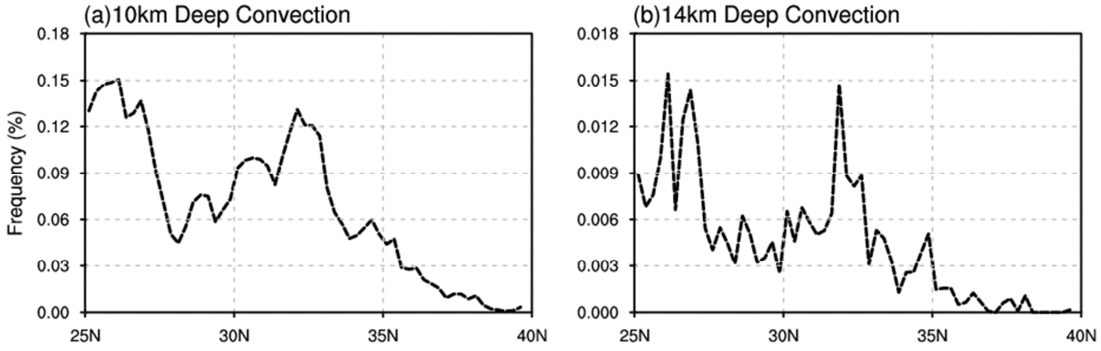

Figure 4. *Zonal mean of deep convection frequencies.*

The above results has shown the different characteristic changes between two types of deep convection. Furthermore, to analyze quantitatively the proportions of the deep convection with different storm top altitudes, the probability density functions (PDF) are conducted in Figure 5. The PDF of storm top altitudes for all deep convective precipitation at each 500m bin of altitude in June, July and August are shown in Figure 5a, Figure 5b and Figure 5c, respectively. The PDF of deep convection, which only occurs over the Tibetan Plateau in summer, is presented in Figure 5d. With the increase of the altitude of storm top, the proportions of various deep convection in all months show a trend of declining

exponentially. Besides, the ratio of deep convection more than 16 km is very small, and the convection of 16 km and above has not appeared in June. This is because the summer monsoon is in the development stage and it cannot produce stronger deep convection.

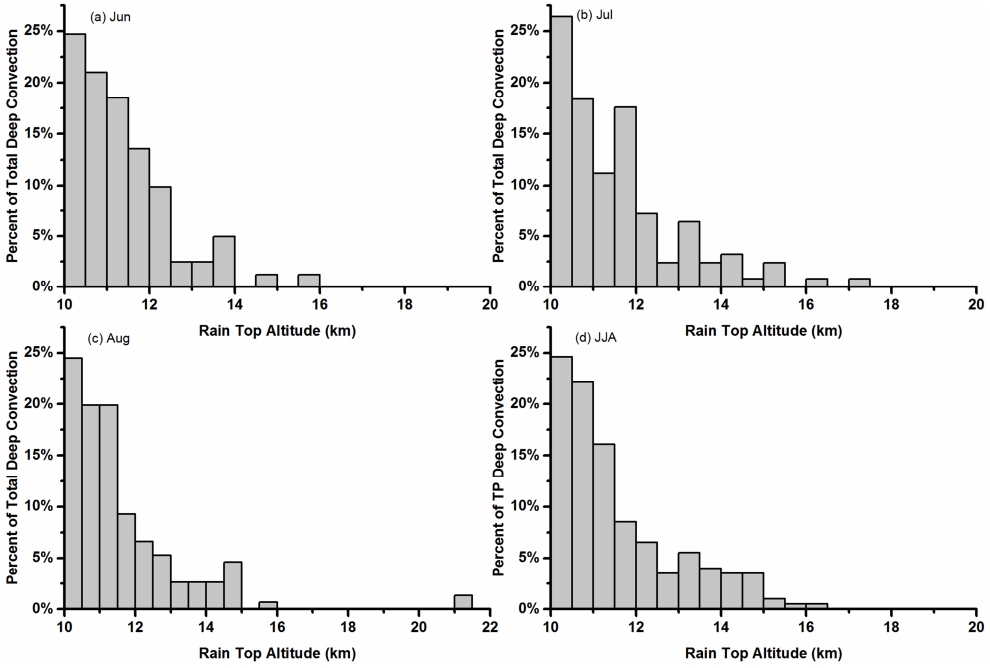

Figure 5. *PDF of deep convections in June (a), July (b), August (c), and JJA (d) over the Tibetan Plateau and surrounding region.*

It has been found that the contribution of frequency of convective precipitation to total precipitation is not more than 30% over the most of southern China during the summer [33]. Expecting to assess the contribution of convective precipitation over the Tibetan Plateau accurately, Figure 6 shows the proportion of convective precipitation to total rain and rain frequency. It is clearly seen from Figure 6 that the contribution of convective precipitation to total rain is consistent with the contribution to rain frequency, and both of the area fractions decrease rapidly with the increasing of contribution. If the contribution is dominant, the proportion of the area fraction is relatively small. In addition, it is worth noting that the maximum contribution of both is below 40%.

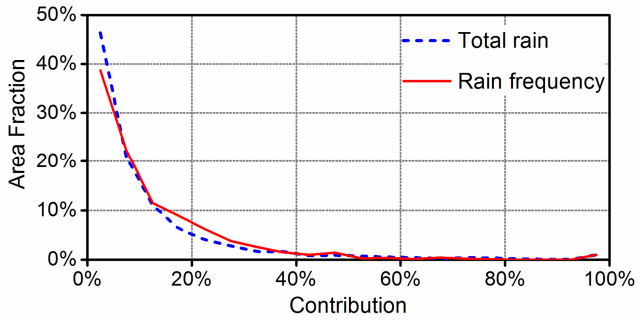

Figure 6. *Area fraction of deep convective precipitation's contributions to total rain and rain frequency.*

3.3. Vertical Profiles of Convective Precipitation

The vertical distribution of rain rates retrieved from echo signal that is observed by DPR at different altitudes, referred to as the precipitation profile, can directly show the vertical structural characteristics of precipitation. Actually, the precipitation profile is able to reflect the thermal-dynamic structure and the micro-processes characteristics [34]. For example, the increase (decrease) of the precipitation intensity is resulted by the growing (breaking, evaporating) in the descending process of the precipitation particles [35-36]. For the same type of precipitation (convective, stratiform or "others"), the average precipitation profiles are still similar even if the surface rain rates are different. Figure 7 shows the mean precipitation profiles and reflectivity profiles detected by GPM DPR in summer. To minimize the surface contamination for radar data and eliminate the effect of terrain height over the Tibetan Plateau, the precipitation profiles below 6 km are not presented in this figure. The average profile (Figure 7a) of convective precipitation indicates that the precipitation clouds are deep, because the storm top can reach 12 km～16 km. At the same storm top altitude, the rain rate from June to August gradually increases, which corresponds to the development of the Asian summer monsoon. The difference between the precipitation profiles for July and August is smaller than the difference between June and July, which is consistent with the performance of Figure 2. The slopes of the profiles begin to change at around 7 km～8 km, corresponding to the height of frozen layer of convective precipitation. The precipitation profiles also indicate the variation of the storm top altitude: the peak height in June is the lowest at 13.5 km, and the highest in August that can reach above 15 km, and the average profile has the same height as July, closing to 15 km. The change of surface rain rate is similar to that of the storm top altitude. The lowest average rain rate is about 5.2 mm/h in Jun, followed by 9

mm/h in July, and the maximum in August, exceeding 10 mm/h. In addition, the summer average precipitation profile is consistent with the profile in July.

The reflectivity profile of convective precipitation detected by DPR is shown in Figure 7b. It is clear that the height of reflectivity is significantly higher than the height of storm top (Figure 7a). The changes of reflectivity in all months are the same, but the reflectivity in June is evidently lower than the other two months. The average reflectivity profile of the whole summer coincides with July below 11 km, while it is consistent with August above 11 km.

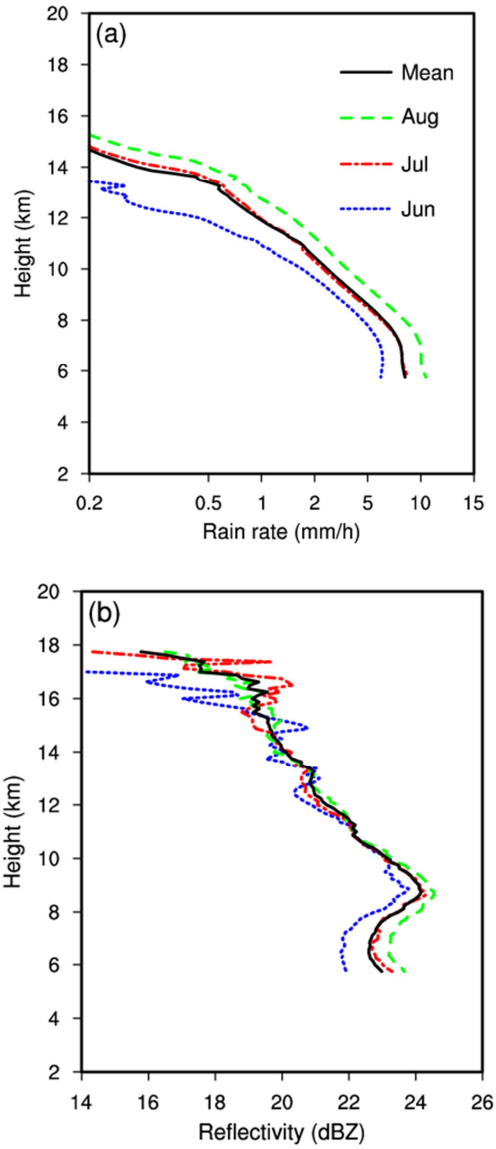

Figure 7. *Mean precipitation profiles and reflectivity profiles of convective precipitation in summer.*

To understand the vertical structure and spatial distribution characteristic of convective precipitation intuitively, Figure 8 presents the average distribution of convective precipitation along the 28°N～35°N. In the area of 80°E～100°E over the Tibetan Plateau, the maximum altitude of storm top can reach 16 km basically, and it rises from west to east. Furthermore, the layer structure of convective precipitation is apparent, and the rain rate shows an obvious gradient change with the increase of height. Below 6 km, rain rate in most areas are above 2 mm/h, and the maximum value can reach 8 mm/h. It is worth nothing that due to the rain rates are averaged over a 9 months of data, so it is still likely that individual storms could contribute to the localized min/maxes. Above 6 km, the precipitation intensity reduced to 4 mm/h and below.

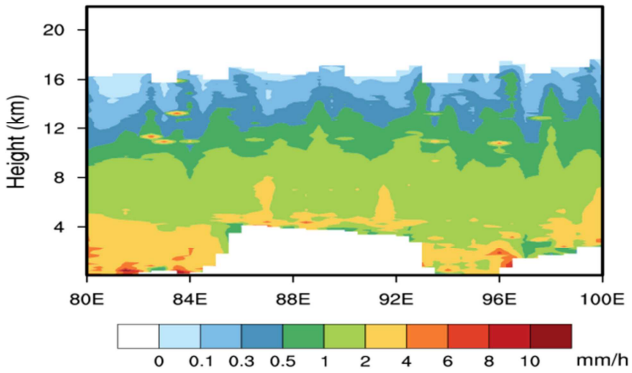

Figure 8. *Height-longitude cross sections of convective rain rate along 28°N～35°N in summer.*

4. Conclusion

The distribution and variation characteristics of convective precipitation over the Tibetan Plateau and its surrounding regions have been paid more and more attention by many scholars. However, due to the scarcity of ground observation stations, the detection data of TRMM PR, which has been stop working, are mainly used in this area. In this study, based on the level-2 precipitation data detected by the GPM DPR, the characteristics of convective precipitation over the Tibetan Plateau and its surrounding regions were analyzed.

The research results show that the number of samples of precipitation with rain top altitude greater than 10 km increase from June to August, and the total number diminishes with the increase of altitude. That is, the higher the storm top altitude, the less the number of precipitation times. The number of precipitation samples with the storm top altitude greater than 10 km over the surrounding regions is always larger than that over the plateau. The frequency of deep convection over the Tibetan Plateau and the surrounding areas is less than 0.8%. The frequency of 14 km deep convection is obviously less than 10 km deep convection, not exceeding 0.2%. With the increase of storm top altitude, the proportion of corresponding deep convection decreases exponentially. The contribution of convective precipitation to total rain and the contribution to total rain frequency are consistent, and both of the area fraction decrease rapidly with the increase of the contribution of convection. The storm top altitude and surface rain rate of convective precipitation are the lowest in June and the highest in August. Furthermore, the storm top altitude over the main body of the TP rises slowly from west to east, and the rain rate shows a significant gradient change with the increase of storm top height.

Acknowledgements

The DPR products were obtained from the Goddard Earth Sciences Data and Information Services Center. All figures were created using the NCAR Command Language (NCL) (2018) (http://www.ncl.ucar.edu). This work was supported by the National Natural Science Foundation of China (41405031, 41475037), the Special Fund for Public Welfare Industry (Meteorology) of China (GYHY201506013), and the Scientific Research Foundation of CUIT (KYTZ201504, J201519).

References

[1] Houze Jr., R. A., Schmid, W., Fovell, R. G., Schiesser, H. H., Hailstorms in Switzerland:left movers, right movers, and false hooks[J]. Mon. Weather Rev. 1993. 121, 3345–3370.

[2] Guo R, Liu Y, Zhou H, et al. Precipitation downscaling using a probability-matching approach and geostationary infrared data: An evaluation over six climate regions [J]. Hydrology & Earth System Sciences Discussions, 2017:1-26.

[3] Arkin, P. A., Ardanuy, P. E. Estimating climatic-scale precipitation from space: A review[J]. J. Clim. 1989, 2, 1229–1238.

[4] Sun Y, Chen Q. Variation of Atmospheric Composition in UTLS during a Strong Convection Process in Tibetan Plateau [J]. Meteorological Science & Technology, 2017.

[5] Sherwood, S. C.; Dessler, A. E. On the control of stratospheric humidity[J]. Geophys. Res. Lett. 2000, 27, 2513-2516.

[6] Li, Q. B.; Jacob, D. J.; Logan, J. A.; Bey, I.; Yantosca, R. M.; Liu, H. Y.; Martin, R. V.; Fiore, A. M.; Field, B. D.; Duncan, B. N.; Thouret, V. Tropospheric Ozone Maximum over the Middle East[J]. Geophys. Res. Lett. 2001, 28, 3235-3238.

[7] Kar, J.; Bremer, H.; Drummond, J. R. Rochon, Y. J.; Jones, D. B.; Nichitu, F.; Zou, J.; Liu, J.; Gille, J. C.; Edwards, D. P.; Deeter, M. N.; Francis, G.; Ziskin, D.; Warner, J. Evidence of vertical transport of Carbon Monoxide from Measurements of Pollution in the Troposphere (MOPITT) [J]. Geophys. Res. Lett. 2004, 31.

[8] Gettleman, A.; Kinnison, D. E. Dunkerton, T. J.; Brasseur, G. P. Impact of Monsoon Circulations on the Upper Troposphere and Lower Stratosphere[J]. J. Geophys. Res. Atmos.2004, 109(D22).

[9] Forster, P. M. D. F., Shine, K. P. Stratospheric water vapor changes as a possible contributor to observed stratospheric cooling[J]. Geophys. Res. Lett. 1999, 26, 3309-3312.

[10] Yang Yuanjian, Yunfei Fu, Fang Qin. Radiative Forcing of the Tropical Thick Anvils Evaluated by Combining TRMM with Atmospheric Radiative Transfer Model，Atmos. Sci. Letter. 2017. 18(5):222-229.

[11] Murakami, M. Analysis of the deep convective activity over the western Pacific and Southeast Asia. Part I: Diurnal variation[J]. J. Meteorol. Soc. Jpn. 1983, 61, 60–76.

[12] Uyeda, H.; Yamada, H.; Horikomi, J.; Shirooka, R.; Shimizu, S.; Liu, L.; Ueno, K.; Fujii, H.; Koike, T. Characteristics of convective clouds observed by a Doppler radar at Naqu on Tibetan Plateau during theGAME-Tibet IOP[J]. J. Meteorol. Soc. Jpn. 2001, 79, 463–474.

[13] Fujinami, H.; Yasunari, T. The seasonal and intraseasonal variability of diurnal cloud activity over theTibetan Plateau[J]. J. Meteorol. Soc. Jpn. 2001, 79, 1207–1227.

[14] Long, Q. C.; Chen, Q. L.; Gui, K.; Zhang, Y. A Case Study of a Heavy Rain over the Southeastern Tibetan Plateau[J]. Atmos. 2016, 7, 118.

[15] Zhong L, Chen L, Yang R, et al. Variability in the vertical structure of precipitation in Sichuan and Chongqing based on 2004-2014 space-borne observations[J]. Acta Meteorologica Sinica, 2018.

[16] Hou, A. Y.; Kakar, R. K.; Neeck, S.; Azarbarzin, A. A.; Kunmmerow, C. D.; Kojima, M.; Oki, R.; Nakamura, K.; Iguchi, T. The global precipitation measurement mission[J]. B. Am. Meteorol. Soc. 2014, 95, 701-722.

[17] Nesbitt, S. W.; Zipser, E. J.; Cecil, D. J. A census of precipitation features in the tropics using TRMM: Radar, ice scattering, and lightning observations [J]. J. Clim. 2000, 13, 4087-4106.

[18] Liu, G.; Fu Y. The characteristics of tropical precipitation profiles as inferred from satellite radar measurements[J]. J. Meteorol. Soc. Jpn. 2001, 79, 131-143.

[19] Fu, Y.; Liu, Y.; Liu, G.; Wang, Q. Seasonal characteristics of precipitation in 1998 over East Asia as derived from TRMM PR[J]. Adv. Atmos. Sci. 2003, 20, 511-529.

[20] Yu, R.; Yuan, W.; Li, J. Fu, Y. Diurnal phase of late-night against late-afternoon of stratiform and convective precipitation in summer southern contiguous China[J]. Clim. Dyn. 2010, 35, 567-576.

[21] Liu, P.; Wang, Y.; Feng, S.; Li, C. Y.; Fu, Y. F. Climatological characteristics of overshooting convective precipitation in summer and winter over the tropical and subtropical regions[J]. Chin. J. Atmos. Sci. 2012, 36, 579-589.

[22] Liu, P.; Li, C. Y.; Wang, Y.; Fu, Y. F. Climatic characteristics of convective and stratiform precipitation over the tropical and subtropical areas as derived from TRMM PR[J]. Sci China Earth Sci. 2012, 42, 1358-1369.

[23] Fujinami, H.; Nomura, S.; Yasunari, T. Characteristics of diurnal variations in convection and precipitation over the southern Tibetan Plateau during summer[J]. Sola. 2005, 1, 49–52.

[24] Fu, Y.; Liu, G.; Wu, G.; Yu, R.; Xu, Y.; Wang, Y.; Li, R.; Liu, Q. Tower mast of precipitation over the central Tibetan Plateau summer[J]. Geophys. Res. Lett. 2006, 33, 157–158.

[25] Yang Yuan-Jian, Da-ren Lu, Yun-Fei Fu, et al., 2015. Spectral Characteristics of Tropical Anvils Obtained by Combining TRMM Precipitation Radar with Visible and Infrared Scanner Data, Pure and Applied Geophysics., 172, (6), 1717-1733 DOI:10.1007/s00024-014-0965-x.

[26] Wang, C.; Shi, H.; Hu, H.; Wang, Y.; Xi, B. Properties of cloud and precipitation over the Tibetan Plateau[J]. Adv. Atmos. Sci. 2015, 32, 1504–1516.

[27] Hamada, A.; Takayabu, Y. N. Improvements in detection of light precipitation with the Global Precipitation measurement dual-frequency precipitation radar (GPM DPR) [J]. J. Atmos. Ocean. Tech. 2016, 33, 653-667.

[28] Beauchamp, R. M.; Chandrasekar, V.; Chen, H.; Vega, M. Overview of the D3R observations during the IFloodS field experiment with emphasis on rainfall mapping and microphysics[J]. J. Hydrometeorology. 2015, 16, 2118-2132.

[29] Skofronick-Jackson, G.; Hudak, D.; Petersen, W. et al. Global Precipitation Measurement Cold Season Precipitation Experiment (GCPEX): For Measurement's sake, Let It Snow[J]. B. Am. Meteorol. Soc. 2015, 96, 1719-1741.

[30] Chandrasekar, V.; Le, M. Evaluation of profile classification module of GPM-DPR algorithm after launch//Geoscience and Remote Sensing Symposium (IGARSS) [J], IEEE International. IEEE, 2015, 5174-5177.

[31] Toyoshima, K.; Masunaga, H.; Furuzawa, F. A. Early evaluation of Ku-and Ka-band sensitivities for the Global Precipitation Measurement (GPM) Dual-Frequency Precipitation Radar (DPR) [J]. SOLA. 2015, 11, 14-17.

[32] Tange, G.; Ma. Y.; Long. D.; Zhong, L.; Hong, L. Evaluation of GPM Day-1 IMERG and TMPA Version-7 legacy products over Mainland China at multiple spatiotemporal scales[J]. J. Hydrometeorology. 2016, 533, 152-167.

[33] Liu, P.; Fu, Y. Climatic characteristics of summer convective and stratiform precipitation in southern China based on measurments by TRMM precipitation radar[J]. Chin. J. Atmos. Sci. 2010, 34, 802-814.

[34] Fujiyoshi, Y.; Takasugi, T.; Gocho, Y.; Takeda, T. Radar-Echo Structure of Middle-Level Precipitating Clouds and the Charge of Raindrops[J]. J. Meteorol. Soc. Jpn. 1980, 58, 203-216.

[35] Hobbs, P. V. Research on clouds and precipitation: Past, present, and future[J]. I. B. Am. Meteorol. Soc. 1989, 70, 282-285.

[36] Zipser, E. J.; Lutz, K. R. The vertical profile of radar reflectivity of convective cells: A strong indicator of storm intensity and lightning probability? [J]. Mon. Weather Rev, 1994, 122, 1751-1759.